

ON THE NATURE OF MAGNETIC SHADOWS IN THE SOLAR CHROMOSPHERE

S. W. MCINTOSH^{1,2} AND P. G. JUDGE³

Received 2001 May 9; accepted 2001 June 29

ABSTRACT

Recent multi-instrument spacecraft studies of the solar photosphere and chromosphere have uncovered a feature—a “magnetic shadow”—not previously discussed in the literature. A region of the mid-chromosphere neighboring, but not within, a network magnetic element exhibits a suppression of both the mean UV line/continuum intensity and the characteristic 3 minute oscillation that is clearly observed elsewhere in apparently similar internetwork regions. The clearest cases appear to occur rarely, and their properties stand in obvious contrast to the well-known “aureoles” of enhanced variability seen surrounding some plage regions. It is imperative to understand more clearly the nature of the shadow region, not least because the suppressed atmospheric heating within it has implications for heating processes elsewhere in the chromosphere that are dependent on, or at least related to, the 3 minute oscillation. Based on the measured photospheric magnetic field, its upward extrapolation, and the appearance of spectral features formed above the midchromosphere, we suggest that a shadow occurs when magnetic structures, in a relatively weak background field, “close” locally within the chromosphere, suppressing the upward propagation of magnetoatmospheric waves into the chromosphere.

Subject headings: Sun: atmospheric motions — Sun: chromosphere — Sun: magnetic fields — Sun: transition region — Sun: UV radiation

1. INTRODUCTION

In a recent paper, Judge, Tarbell, & Wilhelm (2001, hereafter JTW) presented time series observations of the solar photosphere and chromosphere obtained as part of the *Solar and Heliospheric Observatory* (SOHO; Fleck, Domingo, & Poland 1995) and *Transition Region and Coronal Explorer* (TRACE; Handy et al. 1999) Joint Observing Program 72 (“JOP72”). They drew attention to a striking suppression in both the time-averaged and 2–3 minute oscillatory components of the UV continuum intensity at 1195.8 Å, formed in the midchromosphere, observed over an $\sim 10'' \times 10''$ area adjacent to a typical quiet-Sun chromospheric network element with the Solar Ultraviolet Measurement of Emitted Radiation (SUMER) instrument (Wilhelm et al. 1995) on SOHO. JTW noted that this was just the clearest example of several in their data sets. They dubbed this suppression a “magnetic shadow” since the network element appears to “cast a shadow” over the neighboring, also apparently “typical,” internetwork region. The phenomenon is particularly interesting in the light of observations showing enhanced chromospheric and photospheric oscillatory power with 3–5 minute periods in areas, called “aureoles,” that surround plage regions of larger photospheric magnetic flux (see, e.g., Braun et al. 1992 and Brown et al. 1992). Hints of such aureoles have recently been reported in quiet-Sun TRACE UV continuum intensities, formed between the photosphere and the chromosphere, by Krijger et al. (2001). These data, when considered together, suggest that magnetic fields are related either directly or indirectly to the suppression (shadow) or enhancement (aureole) of oscillatory behavior observed in the chromosphere.

¹ High Altitude Observatory, National Center for Atmospheric Research, P.O. Box 3000, Boulder, CO 80307; scott@esa.nascom.nasa.gov.

² European Space Agency, Space Science Department, NASA/Goddard Space Flight Center, Mail Code 682.3, Greenbelt, MD 20771.

³ High Altitude Observatory, National Center for Atmospheric Research, P.O. Box 3000, Boulder, CO 80307; judge@hao.ucar.edu.

It is important to identify the physical nature of magnetic shadows, not only because of their obvious contrast with the aureoles but also because the implied suppression of atmospheric heating in the shadows has consequences for heating processes elsewhere in the chromosphere that depend on, or are at least related to, the dominant 3 minute oscillation. To this end, we reexamine the time series data set examined by JTW that, among the other five discussed by them, most clearly shows the shadow-like behavior. It was obtained on 1999 February 26 between 23:03 and 00:28 UT and is labeled “26 Feb 1999 (II)” by JTW.⁴ To supplement the earlier analysis, we compute potential field extrapolations of data from the Michelson Doppler Imager (MDI; Scherrer et al. 1995) instrument on SOHO and examine the properties of spectral features formed higher than those discussed by JTW. Our aim is to understand the physical differences that can be inferred between the shadow and more typical internetwork regions. We propose that the chromospheric magnetic field topology, estimated using potential field extrapolations, determines the “shadowy” nature of the time-averaged intensity and oscillatory signal observed in the 1999 February 26 (II) JOP72 data.

2. A CLOSER EXAMINATION OF THE 1999 FEBRUARY 26 (II) DATA SET

Figure 1 displays several panels, each providing a close-up of the region containing the shadow in the 1999 February 26 (II) data set. The various quantities are shown as functions of position x along the projected SUMER slit (abscissa, in arcseconds) and time t (ordinate, in minutes). This figure augments those of JTW by including the N I, Si II, and Si III emission-line intensity time series data from SUMER. These lines are formed higher than the 1700 Å (TRACE) and 1195.8 Å (SUMER) continuum data empha-

⁴ Details of the observations (pointing, co-alignment, spectral windows, exposure lengths, etc.) and data reduction are discussed by JTW (their § 2).

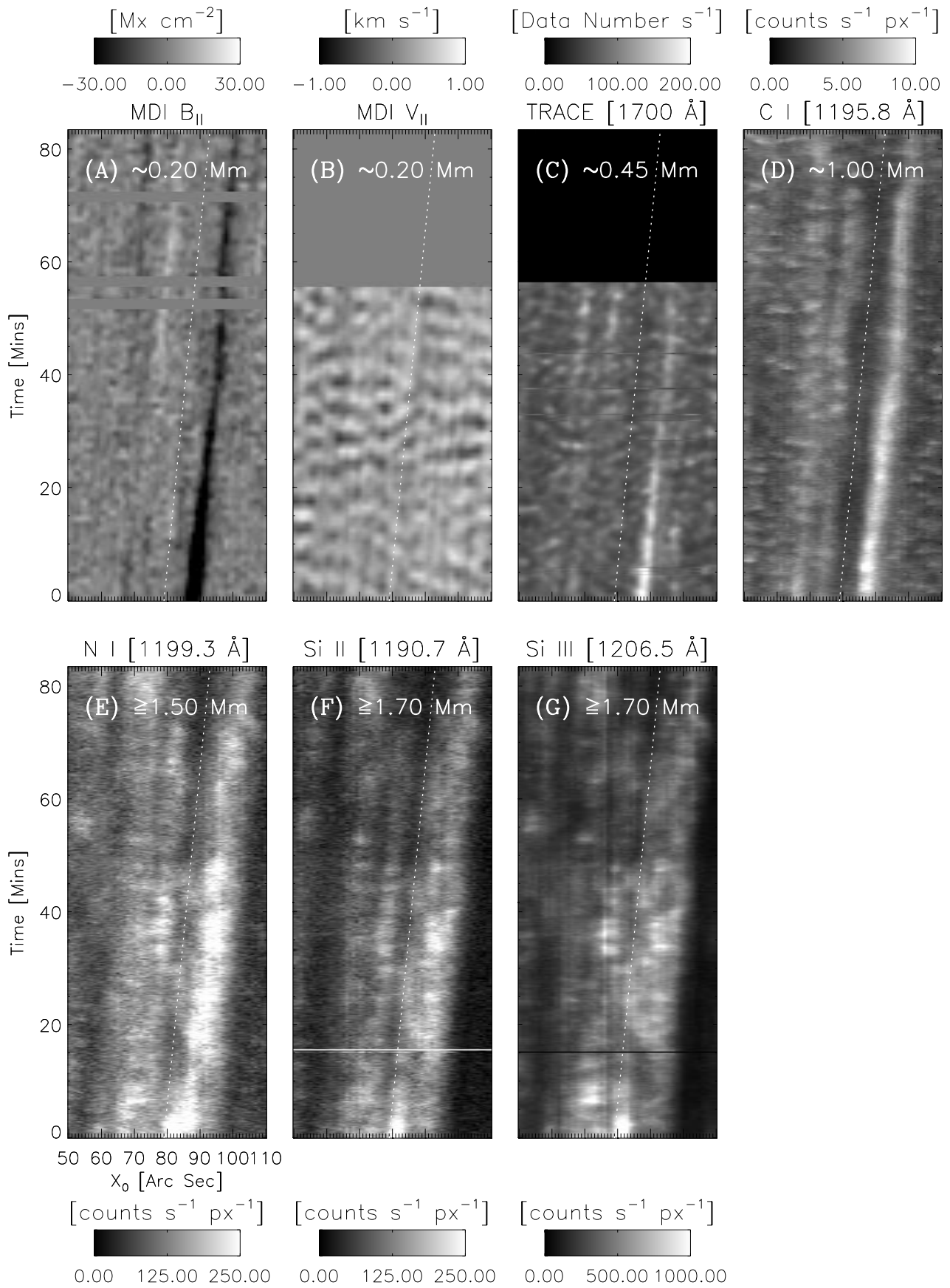


FIG. 1.—Complete set of photospheric ($B_{||}$, $v_{||}$) and UV/EUV 85 minute time series observations for the *SOHO* TRACE JOP 72 on 1999 February 26, as discussed by JTW. In panels (c-f), notice the dramatic reduction in the oscillatory signal, associated with the chromospheric 3 minute oscillation, and line/continuum intensity about spatial position 80. This is the “shadow.” The white dotted line is drawn for reference in each panel, and the approximate formation height of the signal is shown at the top. Notice that the shadow shrinks in spatial extent with height until (g), where it is virtually indistinguishable from the background at or around 1.7 Mm.

sized by JTW. By presenting the observed time series in this way, we can study qualitatively all of the spectral information available, formed from the photosphere (Figs. 1a and 1b) through the low-transition region (Fig. 1g), as discussed in § 3.1 of JTW.

The shadow itself is most clearly seen in the 1195.8 Å continuum time series (Fig. 1d) as the broad, persistently dark feature between $x_0 = 75$ and $x_0 = 85$, immediately to the left of the bright chromospheric network element (the subscript “0” in x_0 refers to the instrument pointing at $t = 0$). This is the location of the shadow as identified by JTW. Indeed, to aid the reader we have placed a light dotted line over the location of the shadow’s apparent center, drawn by eye using Figure 1d, in each of the panels of Figure 1. We note that persistent bright features associated with the magnetic network are all tilted to the right in the figure, and they appear to drift along the SUMER slit. However, this is because solar rotation was not tracked with SUMER, and the *SOHO* spacecraft was rolled by 120° from its normal attitude (for perspective, see Fig. 1 of JTW).

We have scaled the high-resolution MDI magnetogram⁵ of Figure 1a to emphasize the smaller magnetic flux densities than shown by JTW. The MDI sensitivity to longitudinal fields is roughly 10 Mx cm^{-2} in high-resolution mode, so here we set all flux densities with magnitudes below this value to zero to avoid extrapolation of noise. The fields of view (FOVs) of MDI and *TRACE* are larger than that of SUMER, and we show in Figures 1a–1c only those data that underlie the projected position of the $120'' \times 1''$ SUMER slit.

The upper panels show MDI, *TRACE*, and SUMER time series data sets. In particular, they show the line-of-sight (LOS) magnetic flux density B_{\parallel} (Fig. 1a; formed at height $z \approx 0.2 \text{ Mm}$ above the continuum photosphere), LOS velocity v_{\parallel} (Fig. 1b; $z \approx 0.2 \text{ Mm}$), the *TRACE* 1770 Å continuum intensity channel (Fig. 1c; $z \approx 0.45 \text{ Mm}$) and the SUMER C I 1195.8 Å continuum intensities (Fig. 1d; $z \approx 0.7\text{--}1.2 \text{ Mm}$). The most obvious feature in this set of panels is the strong negative polarity flux concentration (with maximum negative flux density of -100 Mx cm^{-2}) between $x_0 = 75$ and $x_0 = 85$, which is associated with the UV-bright network element immediately to the right of the shadow ($x_0 = 86\text{--}91$). Less obvious are several weaker, but real, flux concentrations of both negative and positive polarity between $x_0 = 65$ and $x_0 = 74$, which have associated with them some persistent chromospheric emission (Figs. 1d, 1e, and 1f) and intermittent emission in the *TRACE* 1700 Å channel and the Si III transition region line. It is interesting that there is nothing special about the vertical photospheric motions underlying the shadowed region, as seen in the MDI velocity data (Fig. 1b). Likewise, movies of the full FOV MDI magnetograms show no obvious flux emergence in this region over the duration of the observations.

The lower panels of Figure 1 show additional SUMER observations of the emission lines formed considerably higher than those data shown in the top row: N I 1199.3 Å (Fig. 1e; $z \geq 1.5 \text{ Mm}$); Si II 1190.7 Å (Fig. 1f; $z \geq 1.7 \text{ Mm}$); Si III 1206.5 Å (Fig. 1g; $z \geq 1.7 \text{ Mm}$). These data clearly

show that internetwork oscillations are difficult to see in the emission-line intensities (possible reasons for this are discussed by JTW and McIntosh et al. 2001 and earlier work referenced therein). These data do reveal that the mean intensities of the chromospheric lines (of N I and Si II) appear to be suppressed in a less dramatic manner than, but nevertheless similar to, the 1195.8 Å continuum data of Figure 1d. Thus, the suppressed intensities that partially characterize the shadow can be traced to the highest levels of the chromosphere sampled by these data. The shadow’s intensity signature has essentially disappeared at heights characteristic of the low transition region line of Si III shown in Figure 1g.

Figure 2 shows the spatial variation of the mean intensity $\langle I \rangle$ (Fig. 2, top) and the 3 minute normalized oscillatory power in $\Delta I / \langle I \rangle$ (Fig. 2, middle) and ΔI (Fig. 2, bottom). We compute the oscillatory power as the integral of Fourier

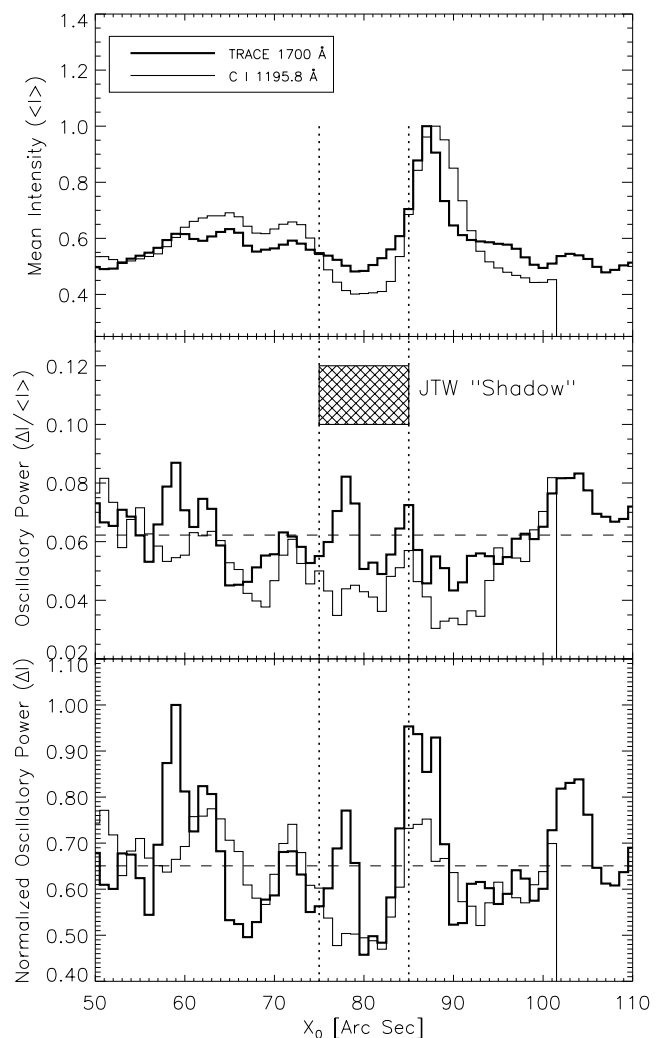


FIG. 2.—Derolled and adjusted (see text) mean intensity $\langle I \rangle$ (top panel) and integrated 3–10 mHz oscillatory power in $\Delta I / \langle I \rangle$ and ΔI (middle and bottom panels, respectively) for the *TRACE* 1700 Å (thick line) and SUMER C I 1195.8 Å continuum (thin line) time series data sets presented in panels c and d, respectively, of Fig. 1. Note the crosshatched area demarking the location of the chromospheric shadow in the SUMER time series and the correlation with the quantities plotted. The average intensity of the C I 1195.8 Å continuum in the shadow region is suppressed by 60% relative to the bright network emission. Similarly, the oscillatory power in the SUMER and (somewhat) in the *TRACE* continua lies below the level of the spatial average (dashed line).

⁵ The MDI instrument, being a photospheric magnetograph, measures a quantity B_{\parallel} that is essentially proportional to $\int \mathbf{B} \cdot d\mathbf{S} / \int d\mathbf{S} \text{ Mx cm}^{-2}$, where \mathbf{B} is the actual field strength vector and $d\mathbf{S}$ is a vector element of area whose plane lies perpendicular to the line of sight.

power at each spatial position over the 3–10 mHz frequency range in both ΔI and $\Delta I/\langle I \rangle$. The raw signals from *TRACE* (Fig. 2, *thick solid line*) and SUMER (Fig. 2, *thin solid line*) are sloped in Figure 1 because of the drift of solar features under the tilted SUMER slit. To derive power spectra, we removed this slope by rotating the original time series, shown in Figures 1c and 1d, by 2° counterclockwise.

The middle and bottom panels of Figure 2 show the signature of the shadow in the 3 minute oscillatory power of the “desloped” time series in $\Delta I/\langle I \rangle$ and ΔI , respectively. McIntosh et al. (2001) made use of the former quantity to assess the degree to which the intensity of the region oscillated, weighted by and relative to $\langle I \rangle$, hence negating the larger network intensities. Here, by using both measures of oscillatory power, we can study the shadow’s degree of relative suppression through $\Delta I/\langle I \rangle$ and absolute suppression through ΔI . In combination, they allow us to completely characterize the shadow whose location, as defined by JTW, is shown.

The dashed line in the bottom and middle panels of Figure 2 shows the spatially averaged oscillatory power in *TRACE* (*thick solid line*). The same quantity for the SUMER data (*thin solid line*) is scaled by a constant factor such that the mean value of the two signals, in each case, is common for the sake of comparison. We see that the oscillatory power in $\Delta I/\langle I \rangle$ is reduced in the network regions ($x_0 = 65\text{--}74$ and $x_0 = 85\text{--}91$), as expected from earlier ground-based analyses (Lites, Rutten, & Kalkofen 1993). It is also clear that the oscillatory power drops significantly below the mean, in $\Delta I/\langle I \rangle$ and ΔI , within the shadow for both the *TRACE* and SUMER time series, rising marginally above the mean only in some narrow regions (e.g., $x_0 = 78$) for *TRACE*. Notice that the overall spatial behavior of the SUMER- and *TRACE*-integrated power spectra is qualitatively similar.

3. PROPOSITION

In summary, the data discussed above show the following. The mean intensity data reveal that the shadow reduces in horizontal extent, with the increasing height of the formation of the spectral feature observed, until it is “filled in” by network transition region emission that is associated with the expanding magnetic fields of the chromospheric network. Chromospheric oscillations, detectable only in the *TRACE* and SUMER 1195.8 Å continuum intensity data, are suppressed throughout the entire region containing a weak network ($65 < x_0 < 74$), a shadow ($75 < x_0 < 85$), and a stronger network ($85 < x_0 < 91$). Since the vertical photospheric motions are similar throughout the entire observed region, we should look for a magnetic origin for the shadow. We propose that magnetic structures that close within the chromosphere are responsible for the shadow phenomenon.

To validate this proposition, we compare the data with potential field extrapolations of the high-resolution MDI magnetograms. While more sophisticated extrapolations using magnetostatic equilibrium calculations (as done by Metcalf et al. 1995), for example, are appealing, not enough is known concerning the gas thermodynamics to make them useful. In addition, the extrapolated chromospheric fields are very sensitive to these unknowns (Solanki & Steiner 1990) and are nonlinear in the magnetic field to an extent that unique extrapolations cannot be guaranteed. By using the potential field approximation, we assume that, while

currents present in the chromosphere will change the field configuration, any gross features of the potential field extrapolations, neighboring source regions of particularly strong photospheric field concentrations, will maintain their overall morphology. In the absence of flux emergence, the potential field extrapolation serves as the simplest reasonable representation of the magnetic field topology throughout the photosphere-chromosphere region.

For each MDI frame, we extract the two-dimensional region surrounding the slit (x - y dimensions $320'' \times 200''$), which we then use as the base ($z = 0$) magnetic field component parallel to the LOS magnetic field [$B_{\parallel}^0 = B_{\parallel}(z = 0)$] to determine a unique three-dimensional Cartesian potential field extrapolation up to a height $z = z_u$ of 5.0 Mm, well above the top of the chromosphere. The transverse components of the extrapolated field at each z [$B_{\perp}(z)$] are computed via the transformation $\hat{B}_{\perp}(z) = K_{\perp} \hat{B}_{\parallel}(z)$, where $\hat{B}_{\parallel}(z)$ represents the two-dimensional fast Fourier transform (FFT) of $B_{\parallel}(z) = B_{\parallel}^0 \exp(-z/H_B)$, with the magnetic scale height H_B set by the physical size of the base pixels ($436 \text{ km} = 0.6''$ for MDI), and K_{\perp} is the matrix whose elements are the wavenumbers corresponding to the (i, j) th coefficient of the two-dimensional FFT. This extrapolation is subject to periodic horizontal boundary conditions and an upper boundary condition that sets field components transverse to the LOS $B_{\perp}(z = z_u)$ to zero.

Figure 3 allows us to compare the extrapolated potential fields with the data of Figures 1 and 2. Figure 3a shows a vertical plane (the x - z plane containing the SUMER LOS) through the extrapolated potential field. Figures 3b–3f exhibit images constructed from the larger FOV MDI (Fig. 3b) and *TRACE* (Figs. 3c–3f) instruments sampling a $120'' \times 20''$ area immediately surrounding the SUMER slit; the latter is marked as a horizontal white line at position $y = 23''$. The image data (Figs. 3b–3d) used here are taken at the midpoint of the time series and have been shifted accordingly, such that the abscissa values are those of x_0 , the initial frame.

As stated above, Figure 3a gives some pictorial details of the extrapolated potential field in the x - z plane containing the SUMER LOS. The thin solid contours indicate lines of constant scalar potential and therefore track representative magnetic field lines. Inspection of these field lines quickly indicates the presence of a quadrupolar field structure in the SUMER LOS spanning positions $x_0 = 65\text{--}88$. The gray scale of this panel gives a measure of the value of $|B| = (B_{\parallel}^2 + B_{\perp}^2)^{1/2}$ in the plane, and we can also see that one side (Fig. 3a, *right*; $x_0 = 74\text{--}88$) of this quadrupolar structure has a larger amount of field associated with it relative to the other. By assuming a background atmosphere that is approximately stratified, as in model VAL3C (see Vernazza, Avrett, & Loeser 1981), we can compute the height z , where the plasma- β ($\beta = 8\pi p_g/B^2$) is 1 (Fig. 3a, *thick white line*) in this plane. We also show a projected closure height of the quadrupolar structure (Fig. 3a, *white cross*) at $x_0 = 72$ and a height of approximately 1.5 Mm.

In Figure 3b we show the (10 Mx cm^{-2} thresholded) MDI high-resolution magnetogram. The negative-positive-negative flux configuration spanning positions 65–88, remarked upon above, is clear. This flux arrangement gives rise to the closed quadrupolar structure of field lines seen in Figure 3a. Figures 3c and 3d show the intensities of *TRACE* 1700 and 1550 Å “C IV” channels at the midpoint of the SUMER time series, respectively. These *TRACE* images are

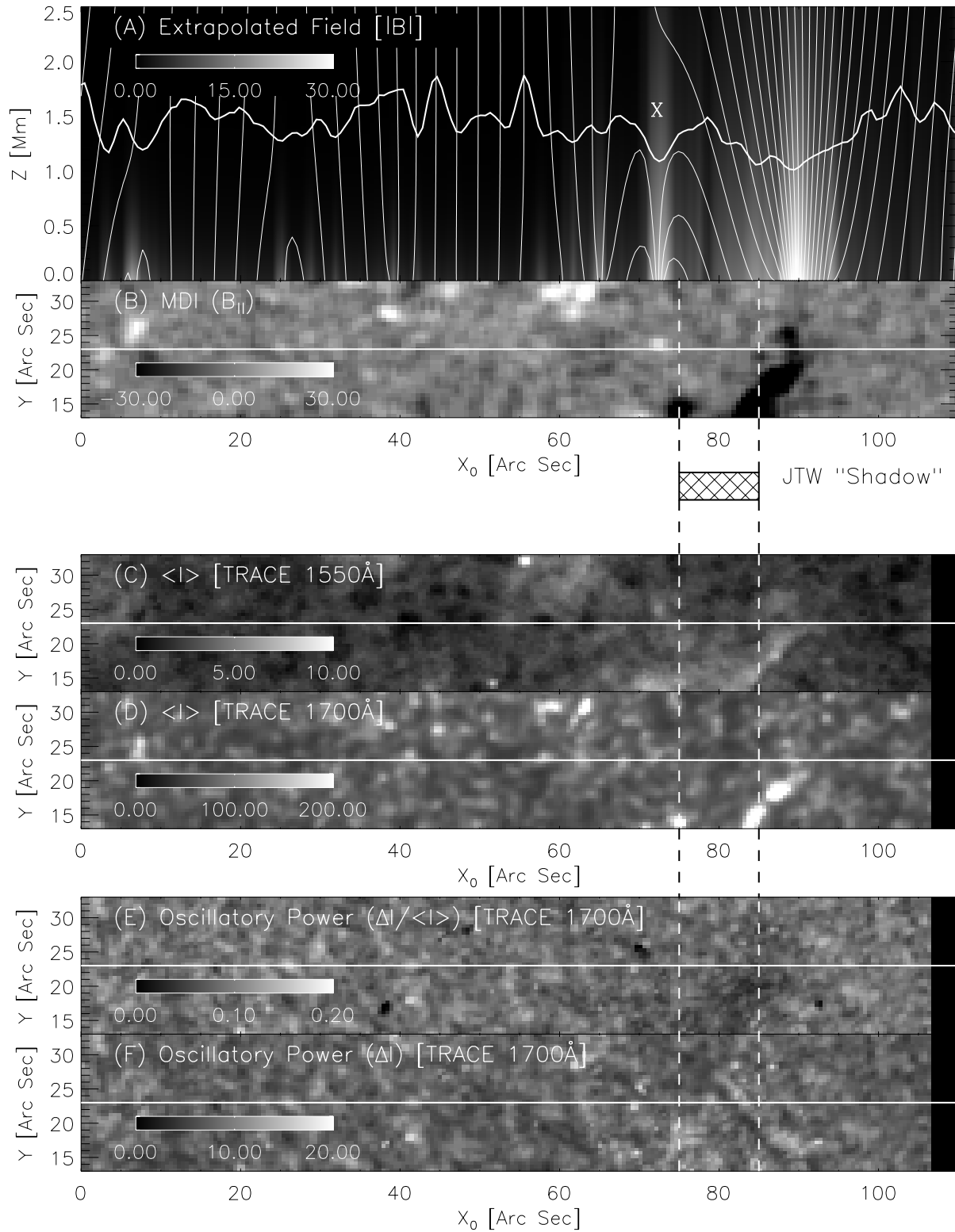


FIG. 3.—(a) Spatial and vertical variation (with a grossly exaggerated vertical scale) of the computed scalar potential in the SUMER LOS plane at the midpoint of the time series. Also shown are lines of constant scalar potential (field lines) in the LOS plane. Notice the quadrupolar “looplike” structure of the field lines around position $x_0 = 74$ in (a). This is the feature we attribute to the observation of the shadow in the panels of Fig. 1. (b–f): Data in the $120'' \times 20''$ region surrounding the SUMER slit (horizontal white line at $y = 23''$) from the larger FOV instruments used (MDI and TRACE). (e, f): Integrated 3–10 mHz oscillatory power of the TRACE 1700 Å channel in $\Delta I / \langle I \rangle$ and ΔI for the same region. The location of the suppressed oscillatory power in the shadow is clear, especially in (e).

constructed by averaging five frames around the time series midpoint to increase the signal-to-noise ratio.

The two-dimensional analog of the lower panels of Figure 2 is shown in Figures 3e and 3f. We compute the 3–10 mHz oscillatory power maps of $\Delta I/\langle I \rangle$ (Fig. 3e) and ΔI (Fig. 3f) for the *TRACE* 1700 Å channel. These maps are constructed from rotation-compensated intensity images to produce power at each pixel in the x - y plane.⁶ It is clear that the 3–10 mHz *TRACE* 1700 Å oscillatory power, in $\Delta I/\langle I \rangle$ and ΔI , is suppressed in the area surrounding the 1195.8 Å shadow relative to the power seen elsewhere in the neighborhood of the SUMER slit. This behavior of the *TRACE* data appears to have no counterpart in the JOP72 data set from 1998 May 12 analyzed by Krijger et al. (2001). In these power maps, the suppressed power characteristic of the shadow extends perhaps through the weak network region to $x_0 = 65$.

Inspection of Figure 3 immediately suggests the following. First, the plasma- β contour lies mostly above 1.2 Mm, the upper limit of the formation height of the 1195.8 Å continuum, except near $x_0 = 73$ and between $x_0 = 83$ and $x_0 = 95$. Thus, if the $\beta = 1$ level contour is the primary determinant of oscillatory behavior everywhere (McIntosh et al. 2001), we would expect to see oscillations everywhere except in these regions. The observations show that this is the case, except in the shadow region. Therefore, suppression of the oscillation within this region requires a different explanation. The striking feature in this figure is that the shadow seems to correspond closely to one of the regions containing fields that close within the chromosphere. This suggests that the quadrupolar magnetic field configuration is somehow responsible for the suppressed oscillation and heating in those regions of the chromosphere, within its closed fields.

Indeed, by focusing on the magnetic data, we suspect that we should redefine the shadow physically to extend beyond the realm previously defined by JTW. We can see from Figures 1, 2, and 3 that a similar shadow-like feature, though far smaller in spatial extent, exists and neighbors the JTW shadow on the left (centered at $x_0 = 70$). This smaller shadow exhibits only a fraction of the intensity suppression and oscillatory power suppression shown in the JTW shadow. From Figures 3a and 3b, it is clear that the left-hand side of the quadrupolar region, spanning $x_0 = 65$ –74, has a qualitatively similar nature to the one causing the JTW shadow. Perhaps the $x_0 = 65$ –74 region has weaker suppression than the JTW shadow ($x_0 = 75$ –85) because the degree of magnetic flux linking the different field concentrations, anchored by the positive flux concentration ($x_0 = 74$), to the left and right is less. This is shown by the gray scale of Figure 3a. The amount of field in the JTW shadow on the right is significantly greater. From this point onward we shall refer to these features together as one *single* shadow.

To test this proposition further, we performed the potential field extrapolation for all of the MDI time series frames covering the SUMER time series. The results are summarized in Figure 4, which shows two loci (*solid white lines*) representing the intersection of two kinds of surface: the $z = 1$ Mm plane, i.e., the approximate height of formation of the C I 1195.8 Å continuum, and the surfaces containing

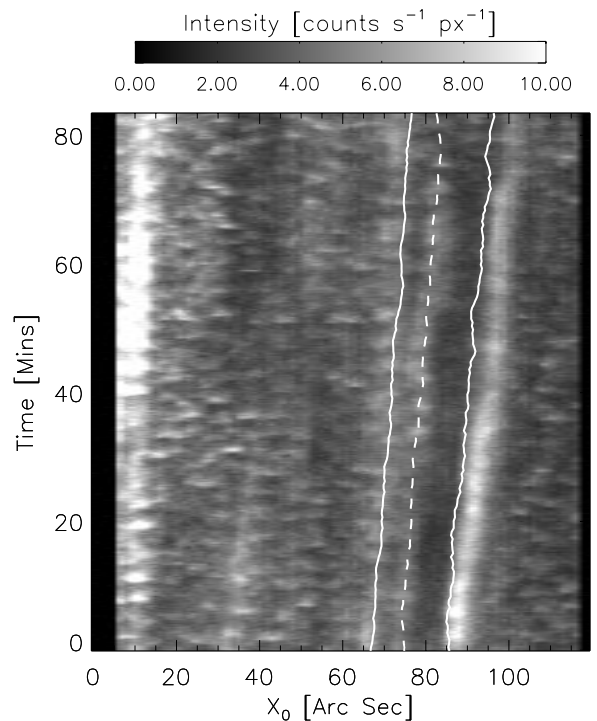


FIG. 4.—*SOHO* SUMER C I 1195.8 Å continuum intensity time series data acquired on 1999 February 26; see Fig. 1d. The data set shows the variation of continuum intensity of a region of atmosphere tracked by the SUMER slit over an 85 minute interval. The solid white lines indicate the positions of the last “open” field lines in the magnetic feature we consider to be responsible for the shadow at the height of formation (~ 1 Mm). We also show the position of the centroid at the same height (*white dashed line*). Notice that the lines follow the features of the shadow well.

the field lines that separate the closed and open magnetic regions. These loci encompass the entire shadow region and are directly related to the distance separating the elements and their relative strength, especially in a region of essentially stationary (flux-emergence-free) quiet-Sun inter-network. The white dashed line shows the position of the center of the positive polarity region, evaluated at $z = 1$ Mm, seen in Figures 3a and 3b.

The observation of a shadow in the quiet-Sun inter-network thus appears to be a consequence of a long-lived element of “return flux” neighboring a stronger network element, which gives rise to a closed-field region within the chromosphere that suppresses both spectral intensities (line and continuum) and the (predominantly 3 minute) chromospheric oscillation.

4. DISCUSSION AND FUTURE WORK

In a nonmagnetic atmosphere, small-amplitude disturbances propagate as acoustic-gravity waves, whose properties have been known for many decades (e.g., Lamb 1932). The solar chromosphere is a more complex medium for wave propagation in several ways. Upward-propagating disturbances rapidly become nonlinear (see, e.g., Carlsson & Stein 1993), and magnetic fields support magneto-atmospheric waves, whose behavior is considerably more complex. For example, the linear problem in homogeneous magnetic fields has received recent attention analytically (Cally 2001), and more complex magnetic geometries have been studied numerically by Rosenthal et al. (2001).

⁶ This method is similar to that presented in Krijger et al. (2001).

The modification of magnetoatmospheric wave modes by magnetic fields can usefully be viewed in terms of the way that the atmosphere is stratified and partitioned by the magnetic field. First, the surface (or surfaces) where the plasma- β is of order unity marks an important transition layer, irrespective of the overall field topology (see, e.g., McIntosh et al. 2001). In predominantly unipolar regions, the locations of $\beta = 1$ isosurfaces in the atmosphere will tend to determine the oscillatory behavior seen in certain spectral features (McIntosh et al. 2001). However, if the atmosphere has regions where mixed magnetic polarity is important, we must also expect the partitioning of the magnetic field into open and closed regions to be critical because certain wave modes are strongly guided by the field lines. Our analysis of *TRACE* and SUMER continua, with field extrapolations from MDI magnetograms, indicates that the latter topological effect is directly responsible for the manifestation of shadows in the SUMER and *TRACE* time series. The differences in the observed intensity/oscillatory power signals appear to be caused by a particular distribution of positive and negative polarity sources of magnetic field at photospheric heights.

Before forming our conclusion, two outstanding points remain: (1) What is the physical mechanism that is responsible for the suppression of the 3 minute oscillation or continuum/line emission within the shadow? (2) Why is the shadow so clearly seen in the 1999 February 26 data and yet has not been clearly seen in other data sets (e.g., Carlsson, Judge, & Wilhelm 1997; Judge, Carlsson, & Wilhelm 1997)?

To answer these questions probably requires detailed MHD simulations, analysis of other joint MDI-SUMER data sets, and perhaps more sensitive magnetic field measurements. These are all beyond the scope of this paper. Concerning point 1 above, while two-dimensional simulations have recently begun under some gross simplifying assumptions concerning the thermodynamics and radiation fields (Rosenthal et al. 2001), these initial calculations have been made for waves with frequencies far above the acoustic cutoff frequency, which is close to that of the dominant observed 3 minute chromospheric oscillation. While some of the properties of these calculations superficially show

encouraging features, we suspect that calculations at lower frequencies are needed that can include the significant dynamic effects of gravity. Concerning point 2, a shadow is not as clearly seen in the companion 1999 February 26 (I) data set, which might be because the 1040 Å continuum is formed too high to clearly see shadows and/or because there is a less mixed polarity field in that particular area under the projected SUMER slit (see Fig. 1 of JTW). JTW speculated that the absence of oscillatory power at 1040 Å throughout the other data set analyzed there—that of 1998 May 16—might arise from magnetic influences from fields whose net flux lies below the detectability limit of MDI. Preliminary comparisons with co-aligned data from the Advanced Stokes Polarimeter obtained by B. W. Lites (2001, private communication) indeed reveal significant amounts of field, including mixed polarities, through much of the region under the projected SUMER slit.

To conclude, the observations of JTW and the presence of the closed magnetic feature in the upward extension of the photospheric magnetic field, which maps out the horizontal position (giving also a reasonable vertical estimate of the height of closure) of the shadow over the entire time series, point to the fact that the particular magnetic configuration—a sufficiently strong photospheric concentration of positive polarity flux lying sufficiently close (~ 10 Mm) to features of opposite polarity—is responsible for the observation of the shadow by SUMER and *TRACE*. Our hope is that careful further analysis of these and similar data sets will help to shed new light on mechanisms responsible for heating the chromosphere both within and outside regions of the chromospheric network.

We are grateful for comments made by Tom Bogdan and Mark Rast during the compilation of this paper. S. W. M. acknowledges the support of the NCAR Advanced Study Program, under which the bulk of this research was carried out, and is currently sponsored by a European Space Agency External Fellowship at the ESA *SOHO* facility (part of the European Solar Magnetometry Network, contract ERBFMRXCT980190) at GSFC. The National Center for Atmospheric Research is sponsored by the National Science Foundation.

REFERENCES

- Braun, D. C., Duvall, T. L., Labonte, B. J., Jefferies, S. M., Harvey, J. W., & Pomerantz, M. A. 1992, *ApJ*, 391, L113
 Brown, T. M., Bogdan, T. J., Lites, B. W., & Thomas, J. H. 1992, *ApJ*, 394, L65
 Cally, P. S. 2001, *ApJ*, 548, 473
 Carlsson, M., Judge, P. G., & Wilhelm, K. 1997, *ApJ*, 486, L63
 Carlsson, M., & Stein, R. F. 1992, *ApJ*, 397, L59
 Fleck, B., Domingo, V., & Poland, A. I. 1995, *The SOHO Mission* (Dordrecht: Kluwer)
 Handy, B. N., et al. 1999, *Sol. Phys.*, 187, 229
 Judge, P. G., Carlsson, M., & Wilhelm, K. 1997, *ApJ*, 490, L195
 Judge, P. G., Tarbell, T. D., & Wilhelm, K. 2001, *ApJ*, 554, 424 (JTW)
 Krijger, J. M., Rutten, R. J., Lites, B. W., Strauss, T., Shine, R. A., & Tarbell, T. D. 2001, *A&A*, submitted
 Lamb, H. 1932, *Hydrodynamics* (New York: Dover)
 Lites, B. W., Rutten, R. J., & Kalkofen, W. 1993, *ApJ*, 414, 345
 McIntosh, S. W., et al. 2001, *ApJ*, 548, L237
 Metcalf, T. R., Jiao, L., McClymont, A. N., Canfield, R. C., & Uitenbroek, H. 1995, *ApJ*, 439, 474
 Rosenthal, C. S., et al. 2001, *ApJ*, in press
 Scherrer, P. H., et al. 1995, *Sol. Phys.*, 162, 129
 Solanki, S. K., & Steiner, O. 1990, *A&A*, 234, 519
 Vernazza, J. E., Avrett, E. H., & Loeser, R. 1981, *ApJS*, 45, 635
 Wilhelm, K., et al. 1995, *Sol. Phys.*, 162, 189